Shell Filling and Trigonal Warping in Graphene Quantum Dots

R. Garreis,[1,*] A. Knothe,[2] C. Tong,[1] M. Eich,[1] C. Gold,[1] K. Watanabe,[3] T. Taniguchi,[3] V. Fal'ko,[2,4] T. Ihn,[1] K. Ensslin,[1] and A. Kurzmann[1]

[1]*ETH Zurich (Swiss Federal Institute of Technology in Zurich), 8093 Zurich, Switzerland*
[2]*National Graphene Institute, University of Manchester, Manchester M13 9PL, United Kingdom*
[3]*National Institute for Material Science, 1-1 Namiki, Tsukuba 305-0044, Japan*
[4]*Henry Royce Institute for Advanced Materials, M13 9PL, Manchester, United Kingdom*

(Received 16 November 2020; accepted 11 March 2021; published 9 April 2021)

Transport measurements through a few-electron circular quantum dot in bilayer graphene display bunching of the conductance resonances in groups of four, eight, and twelve. This is in accordance with the spin and valley degeneracies in bilayer graphene and an additional threefold "minivalley degeneracy" caused by trigonal warping. For small electron numbers, implying a small dot size and a small displacement field, a two-dimensional s shell and then a p shell are successively filled with four and eight electrons, respectively. For electron numbers larger than 12, as the dot size and the displacement field increase, the single-particle ground state evolves into a threefold degenerate minivalley ground state. A transition between these regimes is observed in our measurements and can be described by band-structure calculations. Measurements in the magnetic field confirm Hund's second rule for spin filling of the quantum dot levels, emphasizing the importance of exchange interaction effects.

DOI: 10.1103/PhysRevLett.126.147703

Few-electron quantum dots have been studied in various semiconductors, such as InGaAs [1,2], GaAs [3], InAs [4,5], or silicon [6–8]. Investigation of their ground and excited states, and of their addition spectra led to a comprehensive understanding of orbital and spin degeneracies, and hence enabled the implementation of solid state qubits [9–12]. For vertical quantum dots etched into a circular geometry, shell filling and spin filling according to Hund's rules was observed [1].

A relatively new and promising material for quantum dot qubits is graphene [13]. Almost 99% of the carbon atoms have zero net nuclear spin-reducing hyperfine interactions compared to III-V semiconductors. Furthermore, carbon is a light element with reduced spin-orbit effects even compared to silicon [14]. These properties promise coherence times for qubits in graphene exceeding those of current semiconductor qubits. Because of the recent improvements in fabrication techniques for graphene nanostructures, few electron or few hole quantum dots have been realized in bilayer graphene [15–23] that are comparable in quality to the best devices in GaAs.

However, the quantum dots' ground and excited states, and their addition spectra are not yet fully understood. Charge carriers in large-area bilayer graphene devices possess twofold valley and twofold spin degrees of freedom, as well as a nontrivial minivalley band structure due to trigonal warping [24–27]. Increasing the displacement field perpendicular to the bilayer graphene sheet increases the induced band gap and enhances the depth of the three minivalleys formed around the K and K' points [15,26,27]. Relevance of these minivalleys for low-energy states in quantum dots has so far been predicted only theoretically [28].

Here, we experimentally investigate the effects of trigonal warping in a nearly circular quantum dot in bilayer graphene. Starting from the empty quantum dot we observe a successive bunching of four, eight, and twelve conductance resonances. We attribute these bunchings to the transition from a level scheme given by two-dimensional s and p shells for the first electrons, to a level scheme dominated by minivalleys with threefold degeneracy for more than twelve electrons. Theoretical band-structure calculations confirm this transition and are in good agreement with our experimental observations. The circularity, the size, and the band gap of the quantum dot are calculated using self-consistent COMSOL MULTIPHYSICS simulations for the potential landscape and a capacitive tight-binding model. Measurements in a magnetic field applied parallel to the graphene plane show that spin filling into nearly degenerate levels obey Hund's second rule.

The fabrication of the heterostructure shown schematically in Fig. 1(a) follows the general procedure described in previous publications [15–17,29]. However, here, the thickness of the h-BN layers (bottom, 28 nm; top, 34 nm), the split gate separation (100 nm), the thickness of the aluminium oxide layer (30 nm) as well as the width of the finger gate (20 nm) yield a rather circular shape of the confinement potential as demonstrated later by simulations [see inset Fig. 3(a)]. Figure 1(b) shows a false color atomic force microscope image of the two layers of metal gates fabricated

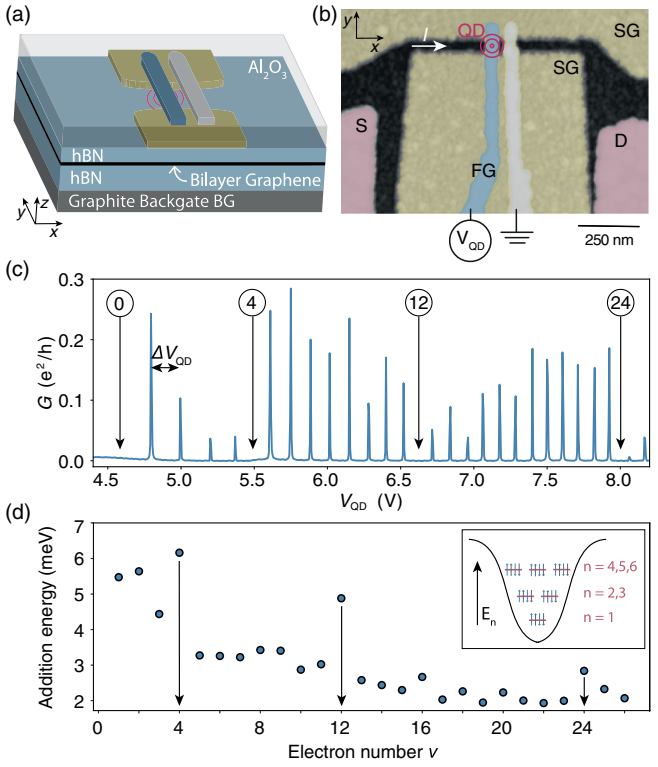

FIG. 1. (a) Schematic representation of the stack. From bottom to top it is built up with a graphite back gate (gray), a bottom *h*-BN (light blue), a bilayer graphene flake capped with a top *h*-BN. Separated vertically by an aluminium oxide layer, the split gates (gold) and finger gate (dark blue) are used to electrostatically define a quantum dot (depicted in red). (b) False color atomic force microscope picture of the sample, with source (S) and drain (D) contacts (rose), split gates (SG, gold) and finger gate (FG, blue). The second finger gate (gray) is grounded. (c) Two-terminal conductance trace through the dot with respect to the applied finger-gate voltage V_{QD}. (d) Addition energy needed for an extra electron versus number of electrons ν in the dot extracted from (b). Inset: Schematic depiction of the potential well including the energy levels n corresponding to the measured bunching, each occupied with four electrons.

on top of the heterostructure. The split gates [golden in Figs. 1(a) and 1(b)] are used to form a conducting channel [black in Fig. 1(b)] [15]. For the measurements discussed in this Letter the right finger gate [gray in Fig. 1(b)] is grounded while the left [blue in Fig. 1(b)] is used to form a quantum dot (QD) underneath it [16,17]. Unless stated otherwise, a *p*-type conducting channel is formed between the two split gates, with insulating regions below them, by applying $V_{BG} = -2.3$ V to the back gate, and $V_{SG} = 1.242$ V to the split gate. The finger gate is then used to form an *n*-type quantum dot, where the *p*-*n* junctions forming between the dot and the channel act as tunnel barriers [16]. Conductance measurements are taken at an electron temperature of ~100 mK by applying a symmetric dc bias of 100 μV and measuring the current in a two-terminal setup.

The single-particle spectrum of this quantum dot is investigated using addition spectroscopy [1,8]. Figure 1(c) shows the conductance through the quantum dot as a function of finger gate voltage V_{QD}. At $V_{QD} = 4.8$ V, the first electron is loaded into the dot, as confirmed with a charge detector neighboring the dot (shown in [18]), and more electrons follow for higher voltages. Bunching of successive Coulomb resonances into groups of four, eight, and twelve is observed. The separation between neighboring Coulomb resonances reflects the energy needed to load the next electron into the dot. In a model based on the Hartree approximation, it is the sum of the charging energy and the separation between the lowest unoccupied and the highest occupied single-particle level [1,16].

With finite bias measurements (presented in Fig. S1 in the Supplemental Material [30]) the finger-gate lever arm $\alpha = 0.027$ is determined for the first electron. It decreases to $\alpha = 0.019$ for the twenty-fourth electron due to increasing dot size. These lever arms allow us to convert the gate voltage differences ΔV_{QD} [horizontal axis of Fig. 1(c)] into energy differences $\Delta E = e\alpha\Delta V_{QD}$ [1]. For the subsequent analysis, the lever arm is determined individually for each electron number.

We plot the addition energy for successive filling of electrons in Fig. 1(d). For the first electron the addition energy is 5.5 meV. It generally decreases with an increasing number of electrons in the dot [1,16], as the electronic size of the dot increases. When the quantum dot is filled with the fourth, the twelfth, and the twenty-fourth electron, an enhanced addition energy is observed, which indicates shell filling in the quantum dot as we will further confirm below [1].

We obtain information about the magnetic properties of the individual single-particle energy levels by measuring their response to an external magnetic field applied perpendicular to the graphene sheet. Subtracting the charging energy between neighboring resonances yields the magnetic field dispersion of the single-particle energy levels E_ν shown in Fig. 2(b) [35]. The two prominent slopes with opposite sign of the levels as a function of $B_\perp$ seen in Fig. 2(b) are well known [16] and reflect the valley splitting due to the opposite magnetization of the K- and K'-valley states. An approximate zero-field single-particle level spacing ΔE_{sp} [Fig. 2(a)] is extracted using the charging energy for each fixed electron number, assuming reasonably that charging energy is independent of the magnetic field [35]. We observe again increased level spacings at four, twelve, and twenty-four electrons, the same as the addition energy in Fig. 1(d), which confirms the shell filling interpretation.

To estimate the circularity of the quantum dot we evaluate its size and shape by solving Poisson's equation in three dimensions with an electron density in the graphene plane determined self-consistently within the Thomas-Fermi approximation. Details of these evaluations are shown in the Supplemental Material [30]. The inset of

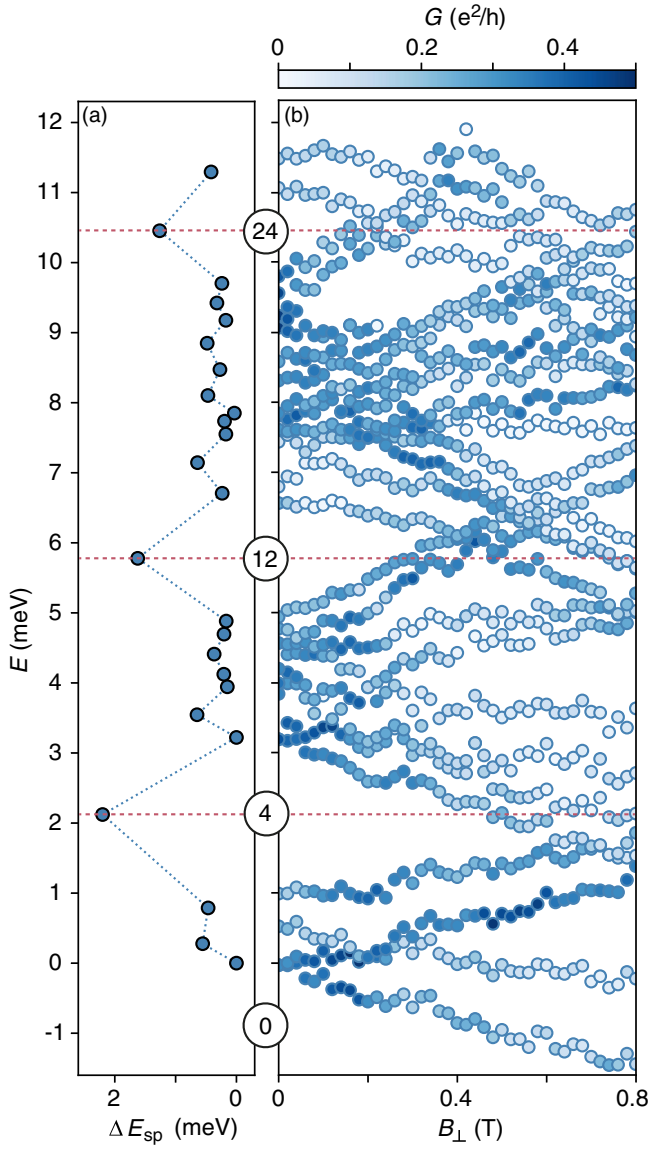

FIG. 2. (a) Single-particle level spacing of the quantum dot as a function of the energy scale extracted from the single-particle energy dispersion in (b) at zero field. The corresponding number of electrons in the dot is marked. (b) Single-particle energy dispersion with perpendicular magnetic field $B_\perp$, taken at $V_{\mathrm{BG}} = -2.5$ V and $V_{\mathrm{SG}} = 1.397$ V.

Fig. 3(a) shows the simulated potential landscape for an exemplary finger gate voltage. The yellow lines outline the split gates forming the conducting channel, where the light blue dashed lines delineate the finger gate that is used to form the dot. Below the finger gate, the higher electric potential forms the potential well serving as the quantum dot confinement potential. The gray lines are equipotential lines indicating the shape of the dot confinement. The nearly circular shape of the equipotentials may cause approximate orbital level degeneracies.

For a comparison of the experimentally determined single-particle level spacing in Fig. 2(a) with the theoretical calculations modeling the system for spinless electrons in a single valley, we plot $E_\nu - E_1$, the single-particle energy levels E_ν with respect to the first energy level E_1, in Fig. 3(a). The measured spectrum shows that the single-particle energies of the first four, fifth to twelfth, and the thirteenth to twenty-fourth electron are each closer together than the energy separation to the next bunch of single-particle energies. This implies that the second and third energy level ($n = 2, 3$) of a given spin and valley are nearly degenerate. The same holds for the fourth, fifth, and sixth levels ($n = 4, 5, 6$) [see inset of Fig. 1(d)].

The threefold degeneracy obtained in the Darwin-Fock model for the third orbital level ($n = 4, 5, 6$) is accidental because of the parabolic confinement potential and cannot explain our observations. In addition, the Berry curvature and the resulting orbital magnetic moment in bilayer graphene lift the degeneracy between d-shell states with different radial quantum numbers [28].

Figures 3(b) and 3(c) show calculated energy levels in a circular bilayer graphene quantum dot for different band gaps inside the dot and different dot sizes, where each data point represents four degenerate spin and valley states. We theoretically describe the quantum dot by a smooth, rotationally symmetric confinement potential with a spatially varying spectral gap (see Supplemental Material for details about the model and the calculation [30]). We model the experiment by simultaneously changing the dot size L and the gap inside the dot (as they are tuned by the finger gate) while keeping the gap under the split gates constant. In Fig. 3(b) we see that for a small dot and a small gap, the dot features a single orbital ground state and orbitally degenerate doublet of excited states, similar to the single-particle level spectrum of a two-dimensional harmonic oscillator. Increasing the dot and gap size in Fig. 3(c) enhances the effect of trigonal warping, leading to triplet degeneracies corresponding to the three minivalleys around each of the bilayer graphene's valleys [see Fig. S2(e) in the Supplemental Material [30]] [28]. Note that the parameters in Figs. 3(b) and 3(c) are chosen, such that we account for the following effects: (1) the electric susceptibility of the bilayer's two monolayers, together with the electron density redistribution between the layers, reduce the value of the gap compared to naive estimates [36]; and (2) an increasing number of electrons inside the dot affect the shape of the confinement potential, causing it to be flatter and more shallow than that for the empty dot. In the Supplemental Material [30], we show further dot spectra for a broader range of parameters, demonstrating that the change of the dot levels' multiplicity with gap and dot size is robust and does not depend on the exact choice of parameters.

Comparing the measured single-particle level spectrum in Fig. 3(a), where groups of four experimental data points correspond to one fourfold degenerate calculated data point in Figs. 3(b) and 3(c) [note that the first two data points in

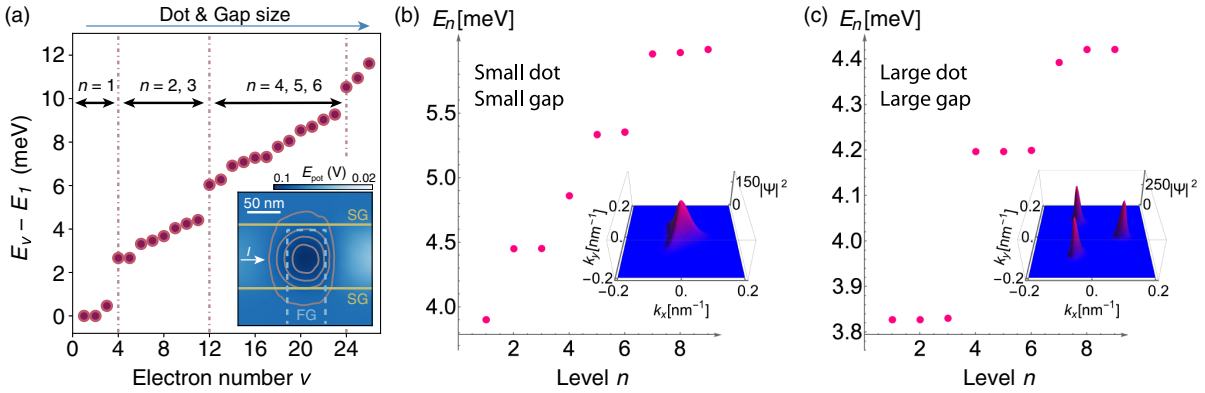

FIG. 3. (a) Single-particle energy levels extracted from Fig. 2. The measured spectrum shows that the second and third ($n = 2, 3$) energy levels are nearly degenerate. The same holds true for the fourth, fifth, and sixth levels ($n = 4, 5, 6$). Inset: Potential landscape induced to the bilayer graphene to form a quantum dot, where $V_{QD} = 6.3$ V, calculated with COMSOL MULTIPHYSICS. (b),(c) Calculated quantum dot spectra for a theoretical model of a rotationally symmetric quantum dot (each level fourfold degenerate in the spin and valley degree of freedom). With increasing dot and gap size, multiplicity of the levels changes and orbital triplet degeneracies emerge due to the three minivalleys around each of bilayer graphene's valleys. Values for small (large) dot and gap sizes for the calculations were chosen to be similar to the experimentally determined values. Furthermore, Fig. S3 in the Supplemental Material shows the robustness of this transition over a wide range of parameters [30]. The insets show the momentum space probability distribution of the lowest dot state in the K^+ valley.

Fig. 3(a) overlap] with the theoretical model, the observed formation of the first two bunches of four and eight levels [see also Fig. 2] agrees with the scenario in Fig. 3(b) of a small dot with a small gap. This scenario, however, does not predict the third bunch of twelve resonances observed in Fig. 2; instead it foresees another two bunches of four and eight resonances, which is not observed. However, since both the displacement field and the quantum dot size increase with increasing electron number in the dot [30], the large-dot-large-gap scenario depicted in Fig. 3(c) explains the bunching of twelve levels. This suggests a gradual transition from the scenario shown in Figs. 3(b) to that in Figs. 3(c) [28] while the quantum dot is being filled with more than five electrons. Such a transition is plausible for the following experimental reasons: First, charging energies extracted from finite-bias Coulomb-diamond measurements decrease consistently with increasing electron number [30], indicating the increasing electronic size of the quantum dot. Second, given the negative back gate voltage in our experiment, an increasingly positive voltage V_{QD} on the finger gate increases the displacement field and thereby the induced band gap inside the quantum dot.

Next, we extract the spin-filling sequence of the quantum dot and the Zeeman splitting of the levels by performing measurements in magnetic field applied parallel to the graphene plane. Figure 4(a) shows the first bunch of four Coulomb peaks with parallel magnetic field. The dashed red lines provide a guide to the eye for a spin splitting with g factor of 2. In agreement with our earlier work [19], we find in Fig. 4(a) that the second electron is filled with its spin parallel to the first, indicating a two-electron spin-triplet and valley-singlet ground state. The third and fourth electrons are then filled with spin opposite to the first two, resulting in a filled shell with zero spin for four electrons in the dot. The observed spin-filling sequence can therefore be characterized by the total-spin quantum number sequence $s_z = 1/2, 1, 1/2, 0$, which follows Hund's second rule.

Similarly, Fig. 4(b) displays the magnetic field dependence of the fifth to twelfth conductance resonance corresponding to the second bunch of levels, i.e., the second

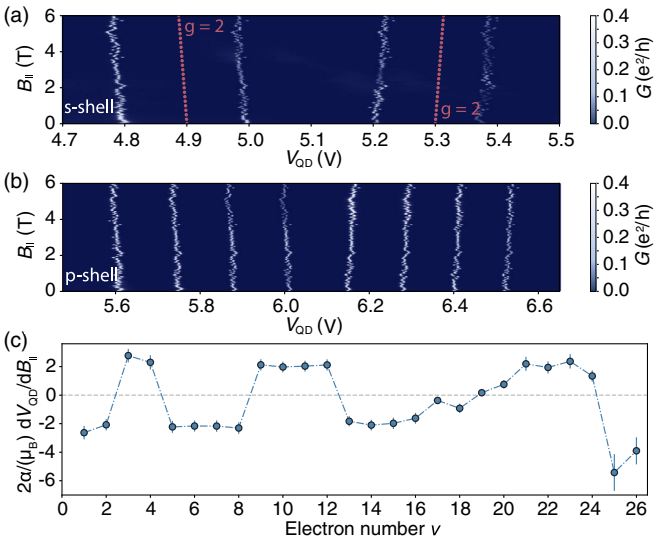

FIG. 4. (a),(b) Conductance through the quantum dot with respect to parallel magnetic field $B_{||}$ and V_{QD} for the first four and the fifth to twelfth electron, respectively. The red lines denote the slope of a Zeeman splitting with a g factor of two for free electrons. (c) Fitted slopes of the shift of the resonances with magnetic field $\alpha/(2\mu_B) dB_{||}/dV_{QD}$. The energy levels ν are filled following Hund's second rule.

shell. The first four electrons loaded into the quantum dot have the same spin, whereas the fifth to the eighth electrons are filled with the opposite spin. The total-spin quantum number sequence in this shell is therefore $s_z = 1/2, 1, 3/2, 2, 3/2, 1, 1/2, 0$. The appearance of the remarkably high total spin $s_z = 2$ for eight electrons in the dot shows that exchange interaction effects are stronger in this quantum dot than any level splittings induced by, for example, deviations from perfect circular symmetry or band nonparabolicities.

Figure 4(c) shows the fitted slopes of shifts of the resonances in magnetic field $2\alpha/\mu_B \times dV_{\mathrm{QD}}/dB_{\parallel}$ which supports this interpretation. Furthermore, we extract g factors from splittings of neighboring peaks [30,37]. For the first twelve electrons, the g factor $|g| = 2.3 \pm 0.3$ fits the expectation for electrons in graphene for small gap sizes and small dots. For larger electron numbers the situation is more complex. In Fig. 4(c) we see that slopes tend to be smaller than the expected values of ± 2, and there is a gradual change of slope from negative to positive values rather than an abrupt jump after the first six filled spins, which would correspond to a half-filled shell. While the exact origin of this behavior remains an open question, we speculate that exchange and correlation effects may play important roles in its explanation.

In summary, we performed measurements on a nearly circular dot, enabling us to observe the transition from filling 1×4- and 2×4-fold degenerate Fock-Darwin-like shells, to filling a 3×4-fold degenerate shell governed by the threefold minivalley symmetry. Observation of this transition was realized by increasing electron occupation of the dot, which is naturally accompanied with an increasing dot size and an increasing band gap. We confirmed that the dot has a nearly circular shape by supporting electrostatic simulations of the potential landscape. Calculations of the single-particle level spectrum of a dot with circular symmetry are in qualitative agreement with our experimental results. Understanding the single-particle spectrum and its tunability is an important step toward identifying suitable states for qubit operation in bilayer graphene quantum dots.

We thank P. Märki and T. Bähler as well as the FIRST staff for their technical support. We thank B. Kratochwil for his support with data analysis. We acknowledge funding from the Core3 European Graphene Flagship Project, the Swiss National Science Foundation via NCCR Quantum Science and Technology, the EU Spin-Nano RTN network, the European Quantum Technology Project 2D-SIPC, the ERC Synergy Grant No. Hetero2D, EPSRC Grants No. EP/S030719/1 and No. EP/N010345/1 and the European Unions Horizon 2020 research and innovation programme under the Marie Skłodowska-Curie Grant Agreement No. 766025. Growth of hexagonal boron nitride crystals was supported by the elemental Strategy Initiative conducted by the MEXT, Japan and JSPS KAKENHI Grant No. JP15K21722.

*garreisr@phys.ethz.ch

[1] S. Tarucha, D. G. Austing, T. Honda, R. J. van der Hage, and L. P. Kouwenhoven, Shell Filling and Spin Effects in a Few Electron Quantum Dot, Phys. Rev. Lett. **77**, 3613 (1996).
[2] L. P. Kouwenhoven, D. G. Austing, and S. Tarucha, Few-electron quantum dots, Rep. Prog. Phys. **64**, 701 (2001).
[3] M. Ciorga, A. S. Sachrajda, P. Hawrylak, C. Gould, P. Zawadzki, S. Jullian, Y. Feng, and Z. Wasilewski, Addition spectrum of a lateral dot from Coulomb and spin-blockade spectroscopy, Phys. Rev. B **61**, R16315 (2000).
[4] I. Shorubalko, A. Pfund, R. Leturcq, M. T. Borgstrm, F. Gramm, E. Mller, E. Gini, and K. Ensslin, Tunable few-electron quantum dots in InAs nanowires, Nanotechnology **18**, 044014 (2006).
[5] A. Fuhrer, L. E. Frberg, J. N. Pedersen, M. W. Larsson, A. Wacker, M.-E. Pistol, and L. Samuelson, Few electron double quantum dots in InAs/InP nanowire heterostructures, Nano Lett. **7**, 243 (2007).
[6] L.-W. Wang and A. Zunger, Dielectric Constants of Silicon Quantum Dots, Phys. Rev. Lett. **73**, 1039 (1994).
[7] D. Culcer, L. Cywiński, Q. Li, X. Hu, and S. D. Sarma, Realizing singlet-triplet qubits in multivalley Si quantum dots, Phys. Rev. B **80**, 205302 (2009).
[8] R. C. C. Leon, C. H. Yang, J. C. C. Hwang, J. C. Lemyre, T. Tanttu, W. Hunag, K. W. Chan, K. Y. Tan, F. E. Hudson, K. M. Itoh, A. Morello, A. Laucht, M. Pioro-Ladrire, A. Saraiva, and A. S. Dzurak, Coherent spin control of s-, p-, d- and f-electrons in a silicon quantum dot, Nat. Commun. **11**, 797 (2020).
[9] D. Loss and D. P. DiVincenzo, Quantum computation with quantum dots, Phys. Rev. A **57**, 120 (1998).
[10] X. Zhang, H.-O. Li, K. Wang, G. Cao, M. Xiao, and G.-P. Guo, Qubits based on semiconductor quantum dots, Chin. Phys. B **27**, 020305 (2018).
[11] K. Wang, H.-O. Li, M. Xiao, G. Cao, and G.-P. Guo, Spin manipulation in semiconductor quantum dots qubit, Chin. Phys. B **27**, 090308 (2018).
[12] D. Cogan, O. Kenneth, N. H. Lindner, G. Peniakov, C. Hopfmann, D. Dalacu, P. J. Poole, P. Hawrylak, and D. Gershoni, Depolarization of Electronic Spin Qubits Confined in Semiconductor Quantum Dots, Phys. Rev. X **8**, 041050 (2018).
[13] B. Trauzettel, D. V. Bulaev, D. Loss, and G. Burkard, Spin qubits in graphene quantum dots, Nat. Phys. **3**, 192 (2007).
[14] H. Min, J. E. Hill, N. A. Sinitsyn, B. R. Sahu, L. Kleinman, and A. H. MacDonald, Intrinsic and Rashba spin-orbit interactions in graphene sheets, Phys. Rev. B **74**, 165310 (2006).
[15] H. Overweg, H. Eggimann, X. Chen, S. Slizovskiy, M. Eich, R. Pisoni, Y. Lee, P. Rickhaus, K. Watanabe, T. Taniguchi, V. Falko, T. Ihn, and K. Ensslin, Electrostatically induced quantum point contacts in bilayer graphene, Nano Lett. **18**, 553 (2018).
[16] M. Eich, R. Pisoni, H. Overweg, A. Kurzmann, Y. Lee, P. Rickhaus, T. Ihn, K. Ensslin, F. Herman, M. Sigrist, K. Watanabe, and T. Taniguchi, Spin and Valley States in Gate-Defined Bilayer Graphene Quantum Dots, Phys. Rev. X **8**, 031023 (2018).
[17] L. Banszerus, B. Frohn, A. Epping, D. Neumaier, K. Watanabe, T. Taniguchi, and C. Stampfer, Gate-defined

electron–hole double dots in bilayer graphene, Nano Lett. **18**, 4785 (2018).

[18] A. Kurzmann, H. Overweg, M. Eich, A. Pally, P. Rickhaus, R. Pisoni, Y. Lee, K. Watanabe, T. Taniguchi, T. Ihn, and K. Ensslin, Charge detection in gate-defined bilayer graphene quantum dots, Nano Lett. **19**, 5216 (2019).

[19] A. Kurzmann, M. Eich, H. Overweg, M. Mangold, F. Herman, P. Rickhaus, R. Pisoni, Y. Lee, R. Garreis, C. Tong, K. Watanabe, T. Taniguchi, K. Ensslin, and T. Ihn, Excited States in Bilayer Graphene Quantum Dots, Phys. Rev. Lett. **123**, 026803 (2019).

[20] L. Banszerus, S. Möller, E. Icking, K. Watanabe, T. Taniguchi, C. Volk, and C. Stampfer, Single-electron double quantum dots in bilayer graphene, Nano Lett. **20**, 2005 (2020).

[21] M. Eich, R. Pisoni, C. Tong, R. Garreis, P. Rickhaus, K. Watanabe, T. Taniguchi, T. Ihn, K. Ensslin, and A. Kurzmann, Coulomb dominated cavities in bilayer graphene, Phys. Rev. Research **2**, 022038(R) (2020).

[22] L. Banszerus, A. Rothstein, T. Fabian, S. Möller, E. Icking, S. Trellenkamp, F. Lentz, D. Neumaier, K. Watanabe, T. Taniguchi, F. Libisch, C. Volk, and C. Stampfer, Electron–hole crossover in gate-controlled bilayer graphene quantum dots, Nano Lett. **20**, 7709 (2020).

[23] C. Tong, R. Garreis, A. Knothe, M. Eich, A. Sacchi, K. Watanabe, T. Taniguchi, V. Fal'ko, T. Ihn, K. Ensslin, and A. Kurzmann, Tunable valley splitting and bipolar operation in graphene quantum dots, Nano Lett. **21**, 1068 (2021).

[24] E. McCann, D. S. Abergel, and V. I. Fal'ko, The low energy electronic band structure of bilayer graphene, Eur. Phys. J. Special Topics **148**, 91 (2007).

[25] D. Xiao, M.-C. Chang, and Q. Niu, Berry phase effects on electronic properties, Rev. Mod. Phys. **82**, 1959 (2010).

[26] A. Varlet, M. Mucha-Kruczyski, D. Bischoff, P. Simonet, T. Taniguchi, K. Watanabe, V. Falko, T. Ihn, and K. Ensslin, Tunable Fermi surface topology and Lifshitz transition in bilayer graphene, Synth. Met. **210**, 19 (2015).

[27] A. Knothe and V. Fal'ko, Influence of minivalleys and Berry curvature on electrostatically induced quantum wires in gapped bilayer graphene, Phys. Rev. B **98**, 155435 (2018).

[28] A. Knothe and V. Fal'ko, Quartet states in two-electron quantum dots in bilayer graphene, Phys. Rev. B **101**, 235423 (2020).

[29] L. Wang, I. Meric, P. Y. Huang, Q. Gao, Y. Gao, H. Tran, T. Taniguchi, K. Watanabe, L. M. Campos, D. A. Muller, J. Guo, P. Kim, J. Hone, K. L. Shepard, and C. R. Dean, One-dimensional electrical contact to a two-dimensional material, Science **342**, 614 (2013).

[30] See Supplemental Material at http://link.aps.org/supplemental/10.1103/PhysRevLett.126.147703 for the simulations and calculations on the potential landscape as well as the dot and gap size, the theoretical model and the calculation of the single-particle level spectrum, and the derivation of the g factor and additional data in the parallel magnetic field not presented in the main text. It includes Refs. [31–34].

[31] E. McCann, Interlayer asymmetry gap in the electronic band structure of bilayer graphene, Phys. Status Solidi (b) **244**, 4112 (2007).

[32] T. Ihn, *Semiconductor Nanostructures: Quantum States and Electronic Transport* (Oxford University Press, New York, 2010).

[33] E. McCann and M. Koshino, The electronic properties of bilayer graphene, Rep. Prog. Phys. **76**, 056503 (2013).

[34] A. Varlet, D. Bischoff, P. Simonet, K. Watanabe, T. Taniguchi, T. Ihn, K. Ensslin, M. Mucha-Kruczyński, and V. I. Fal'ko, Anomalous Sequence of Quantum Hall Liquids Revealing a Tunable Lifshitz Transition in Bilayer Graphene, Phys. Rev. Lett. **113**, 116602 (2014).

[35] D. S. Duncan, D. Goldhaber-Gordon, R. M. Westervelt, K. D. Maranowski, and A. C. Gossard, Coulomb-blockade spectroscopy on a small quantum dot in a parallel magnetic field, Appl. Phys. Lett. **77**, 2183 (2000).

[36] S. Slizovskiy, A. Garcia-Ruiz, N. Drummond, and V. I. Falko, Dielectric susceptibility of graphene describing its out-of-plane polarizability, arXiv:1912.10067.

[37] S. Lindemann, T. Ihn, T. Heinzel, W. Zwerger, K. Ensslin, K. Maranowski, and A. C. Gossard, Stability of spin states in quantum dots, Phys. Rev. B **66**, 195314 (2002).